2010 International Conference on Pattern Recognition

# Live Cell Segmentation in Fluorescence Microscopy via Graph Cut

Milán Leskó, Zoltan Kato, Antal Nagy
*Department of Image Processing and Computer Graphics, University of Szeged, H-6701 Szeged, PO. Box 652., Hungary*
*Lesko.Milan@stud.u-szeged.hu,{kato,nagya}@inf.u-szeged.hu*

Imre Gombos, Zsolt Török, László Vígh Jr, László Vígh
*Molecular Stress Biology Group, Institute of Biochemistry, Biological Research Center, Hungarian Academy of Sciences*
*{gombosi,tzsolt,vigh}@brc.hu,Vigh.Laszlo@stud.u-szeged.hu*

***Abstract*—We propose a novel Markovian segmentation model which takes into account edge information. By construction, the model uses only pairwise interactions and its energy is submodular. Thus the exact energy minima is obtained via a max-flow/min-cut algorithm. The method has been quantitatively evaluated on synthetic images as well as on fluorescence microscopic images of live cells.**

## I. Introduction

Image segmentation in biomedical imaging is aiming to find boundaries of various biological structures such as cells, chromosomes, genes, proteins and other sub-cellular components [1], [2], [3]. Due to the highly complex structures, semi-automatic (or interactive) methods allowing for a minimal user interaction are preferable as the identification of foreground regions requires expert knowledge. Classical solutions, *e.g. Cellprofiler* [4], adopts either global or adaptive thresholding followed by a watershed method for separating adjacent regions. Fluorescence microscopy is a low light imaging technique broadly used in live cell experiments. Segmentation of such images require sophisticated methods as this imaging technique is producing noisy, blurred and low contrast images.

Markov Random Fields (MRF) provide a powerful tool to construct segmentation models of degraded images yielding an energy minimization problem. Unfortunately, the exact minimization of a general energy function is NP-hard, requiring iterative algorithms [5], which is a major obstacle for adopting MRF models in interactive segmentation. However, certain class of energy functions can be exactly minimized by graph cuts in *polynomial time* [6].

Herein, we propose an interactive segmentation algorithm in which a user indicates (*e.g.* by free-hand painting) an initial set of pixels as foreground and background. Our method uses this input, along with a set of gradient vectors, to initialize an MRF. The optimal foreground/background assignment is then obtained via graph cut [7]. The minimal cost for the underlying MRF can be found in real time thus allowing interactive adjustments by adding additional patches of foreground or background. The main contribution is the efficient use of the full gradient information (*i.e.* both magnitude and direction) in our MRF model without compromising the ability to find an exact solution via graph cut. The proposed method has been validated on both synthetic and real microscopic images. Comparative results with classical MRF models confirmed the increased segmentation accuracy of the proposed approach.

Supported by the grant CNK80370 of the National Office for Research and Technology (NKTH) & the Hungarian Scientific Research Fund (OTKA); the TÁMOP-4.2.2/08/1-2008-0014 and TÁMOP-4.2.2/08/1-2008-0005 programs of the Hungarian National Development Agency.

## II. MRF segmentation model

Segmentation can be considered as a labeling problem: Given a set of sites (or pixels) $\mathcal{S} = \{s_1, s_2, \ldots, s_N\} \subset \mathbb{Z}^2$ and observed image features (*e.g.* graylevels) $\mathcal{F} = \{f_s\}_{s\in\mathcal{S}}$, we want to assign a label $\omega_s \in \{0, 1\}$ to each site $s$. Taking a Bayesian approach, we can factorize the posterior as $P(\omega|\mathcal{F}) \propto P(\mathcal{F}|\omega)P(\omega)$, where the optimal segmentation $\widehat{\omega}$ is obtained as the *Maximum a Posteriori* (MAP) estimate. MRFs are broadly used in building probabilistic models for such labeling problems. The *Hammersley-Clifford theorem* provides a convenient way to specify MRFs through clique potentials. It states the equivalence between MRFs and Gibbs fields with probability distribution [5]

$$P(\omega|\mathcal{F}) = \frac{1}{Z}\exp\left(-\sum_{c\in\mathcal{C}} V_c(\mathcal{F},\omega)\right),$$

where $Z$ is the normalizing constant, $\mathcal{C}$ denotes the set of cliques induced by the neighborhood system (see Fig. 1) and $V_c$ stands for the *clique potential* functions. A *clique* is defined as the set of sites in which each site is a neighbor of all the other. The MAP estimate of the hidden *labeling field* $\omega$ is then found by minimizing the Gibbs energy. Herein, we consider 8-neighborhood cliques on the image lattice $\mathcal{S}$, giving rise to cliques up to order 4. However, only pairwise interactions are considered in order to ensure that the Gibbs energy can be minimized via standard max-flow/min-cut [7], [6].

In our case (see Fig. 3), the background/foreground graylevel distributions can be easily modeled as Gaussian densities with parameters $(\mu_\lambda, \sigma_\lambda), \lambda \in \{0, 1\}$. In order to ensure object coherence, $P(\omega)$ is usually chosen to be the *Ising* prior consisting of pairwise clique potentials

$$\forall (s, r) \in \mathcal{C} : \beta\delta(\omega_s, \omega_r) \qquad (1)$$

1051-4651/10 $26.00 © 2010 IEEE
DOI 10.1109/ICPR.2010.367

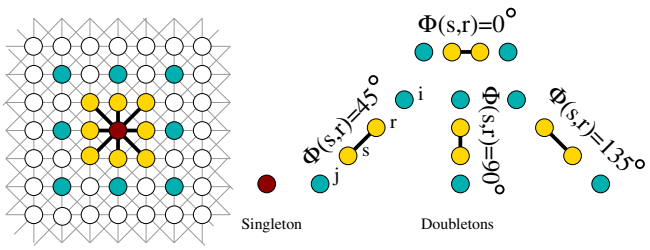


Figure 1. Neighborhood and cliques.

with $\delta(\omega_s, \omega_r) = -1$ for homogeneous and $+1$ for inhomogeneous arguments. Indeed, this prior will enforce homogeneity *everywhere*. A more efficient prior would be to encourage coherence only where intensity gradient is low. The idea of taking into account intensity edges has appeared as early as in [5], while recently, in the context of graph cut, a contrast-sensitive Gaussian Mixture MRF model has been proposed in [8]. However, [5] defines a separate *line process* with higher order interactions which are difficult to handle in a graph-cut framework. On the other hand, [8] uses a so called *contrast* term in the data likelihood, which is related to the squared intensity difference between interacting pixel pairs but ignores gradient direction.

In contrast to previous approaches, we propose to exploit the full gradient information (*i.e.* magnitude and direction) while keeping the ability to find an exact MAP solution via standard max-flow/min-cut. Obviously, the prior cannot depend on the data, hence we have to include the additional gradient terms in our data likelihood. Given the gradient vector field $\nabla\mathcal{F}$ with normalized magnitudes $|\nabla\mathcal{F}(s)| \in [0,1]$ and quantized edge directions $\theta(s) \in \{0°, 45°, 90°, 135°\}$ perpendicular to the gradient direction, we define the gradient strength $M(s,r)$ and edge direction $\Theta(s,r)$ for all doubletons $(s,r) \in \mathcal{C}$ as

$$M(s,r) = \min\{M_{\max}, \\ -\min\{\log(1-|\nabla\mathcal{F}(s)|), \log(1-|\nabla\mathcal{F}(r)|)\}\} \quad (2)$$

$$\Theta(s,r) = \begin{cases} \theta(s) & \text{if } |\nabla\mathcal{F}(s)| > |\nabla\mathcal{F}(r)| \\ \theta(r) & \text{otherwise} \end{cases}$$

where $M_{\max}$ is the maximum allowed value for $M(s,r)$ (*i.e.* we clip $M(s,r)$ at $M_{\max}$). Furthermore, we define an indicator function

$$F(s,r) = H((\mu_{\omega_s} - \mu_{\omega_r})(f_s + f_j - f_r - f_i)), \quad (3)$$

where $H$ is the Heaviside function and the location of sites $j$ and $i$ is shown in Fig. 1. Clearly, $F$ will return 0 whenever the labels $\omega_s$ and $\omega_r$ are on the wrong side of the contour, because in such situations the difference in graylevel values $f_s + f_j$ and $f_r + f_i$ will have an opposite sign than that of the corresponding mean values. This function allows us to enforce object coherence around contours. The new doubleton potential added to the likelihood is then defined as

$$G(s,r) = (1 - F(s,r))\mathcal{M} \\ -F(s,r)H(\delta(\Theta(s,r), \Phi(s,r)))M(s,r) \quad (4)$$

where $\mathcal{M} \gg M_{\max}$ corresponds to a large constant penalty preventing wrong label assignments around object boundaries. Otherwise, the energy is decreased by $M(s,r)$ whenever the edge direction $\Theta(s,r)$ doesn't match with the clique direction $\Phi(s,r)$ (see Fig. 1), meaning that there is an intensity edge passing between $s$ and $r$. The data likelihood MRF energy is then composed of singleton and doubleton potentials as follows

$$U(\mathcal{F},\omega) = \sum_{s\in\mathcal{S}} \log(\sqrt{2\pi}\sigma_{\omega_s}) + \frac{(f_s - \mu_{\omega_s})^2}{2\sigma_{\omega_s}^2} \\ +\alpha \sum_{(s,r)\in\mathcal{C}} H(\delta(\omega_s,\omega_r))G(s,r) \quad (5)$$

Putting together Eq. (1) and Eq. (5), the Gibbs energy to be minimized can be written as

$$\widehat{\omega} = \arg\min_{\omega} \left( U(\mathcal{F},\omega) + \beta \sum_{(s,r)\in\mathcal{C}} \delta(\omega_s,\omega_r) \right) \quad (6)$$

## III. Exact MAP solution via graph cut

Herein, we will show that the Gibbs energy of Eq. (6) can be represented by a graph $\mathcal{G}$ and hence an exact MAP solution is found in polynomial time by computing the minimum *s-t-cut* on $\mathcal{G}$ [6]. The vertices include the terminals $\mathbf{s}$ (*source*) and $\mathbf{t}$ (*sink*) as well as sites $\mathcal{S}$. Since our model uses pairwise interactions and binary labels, it can be naturally translated into a graph representation where, in addition to edges corresponding to doubletons, edges connecting vertices from $\mathcal{S}$ with the terminals $\mathbf{s}$ and $\mathbf{t}$ are also defined (see [6] for details). A cut on $\mathcal{G}$ corresponds to a binary partitioning $S, T$ of the vertices such that $\mathbf{s} \in S$ and $\mathbf{t} \in T$, which can be described by the binary variables $\omega_s, s \in \mathcal{S}$. Each cut has also a cost corresponding to the sum of edge weights that go from $S$ to $T$, thus the energy represented by $\mathcal{G}$ can be seen as a function $E(\omega)$ equal to the cost of the cut defined by $\omega$. In our case, $E(\omega)$ is as follows:

$$E(\omega) = \sum_{s\in\mathcal{S}} E_s(\omega_s) + \sum_{(s,r)\in\mathcal{C}} E_{s,r}(\omega_s,\omega_r), \quad (7)$$

where $E_s$ corresponds to the Gaussian term from Eq. (5), while $E_{s,r}$ includes both the Ising prior and the gradient term of Eq. (5):

$$E_{s,r}(\omega_s,\omega_r) = \beta\delta(\omega_s,\omega_r) + \alpha H(\delta(\omega_s,\omega_r))G(s,r).$$

The main theoretical result of [6] states that a necessary and sufficient condition for graph-representability of $E$ is the following *submodularity* condition:

$$E_{s,r}(0,0) + E_{s,r}(1,1) \leq E_{s,r}(0,1) + E_{s,r}(1,0). \quad (8)$$

It is easily seen that the left hand side is always $-2\beta$ for all $(s,r)$, as the gradient term vanishes. On the right hand side, we have a constant $2\beta$ from the Ising term, $\alpha\mathcal{M}$ from one of the inhomogeneous label configurations and either $0$ or $-\alpha M(s,r)$ from the other depending on the edge direction. Thus for all $(s,r) \in \mathcal{C}$, we have

$$E_{s,r}(0,1) + E_{s,r}(1,0) \geq 2\beta + \alpha(\mathcal{M} - M_{\text{max}})$$

since, according to Eq. (2), $M_{\text{max}} \geq M(s,r)$ always holds. Therefore submodularity is satisfied for $\beta, \alpha > 0$ if

$$-4\frac{\beta}{\alpha} \leq \mathcal{M} - M_{\text{max}},$$

which is always true as we have chosen $\mathcal{M} \gg M_{\text{max}}$.

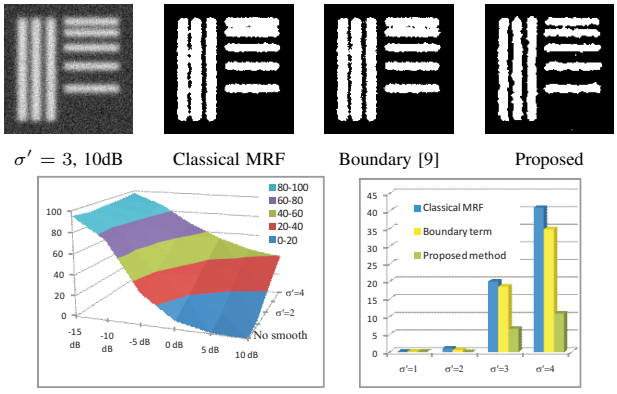


Segmentation error vs. noise and blur — Separation error vs. blur

Figure 2. Results on synthetic images.

## IV. Experimental results

In our experiments, $\nabla\mathcal{F}$ was provided by a Sobel operator followed by non-maxima suppression (see Fig. 3 for a typical gradient image) and we set $M_{\text{max}} = 10^3$ and $\mathcal{M} = 10^6$. Gaussian parameters were learned from user selected input regions (see Fig. 4), while the parameters $\alpha$ and $\beta$ were set to their optimal value. The MAP segmentation was then obtained by the max-flow implementation of Kolmogorov (http://www.cs.ucl.ac.uk/staff/V. Kolmogorov/software.html) [7]. We have also compared results obtained by two classical MRF models: The first one uses an Ising prior (equivalent to removing the gradient term by setting $\alpha = 0$); and 2) a MRF model where the gradient term is replaced by the *boundary term* from [9], which penalizes discontinuities inversely proportional to differences in pixel intensity.

For quantitative evaluation, a set of synthetic images of size $140 \times 140$ has been generated from four binary images by Gaussian smoothing with $\sigma' = \{1,2,3,4\}$ and adding white noise ranging from $-15$dB to 10dB (see Fig. 2). The segmentation error is calculated as the percentage of misclassified pixels. Fig. 2 shows the average error w.r.t. blur and noise. Obviously, error is linearly increasing with $\sigma'$ as blurred regions become bigger. On the other hand, our method is quite robust up to 0dB noise level, but becomes quickly unstable above it. We have also evaluated the separation accuracy of our method on noisy blurred images and found that even for moderate smoothing, it outperforms both classical MRF models. Fig. 2 shows the separation error computed as the percentage of the false foreground pixels in gap areas w.r.t. the total number of pixels of the gap areas.

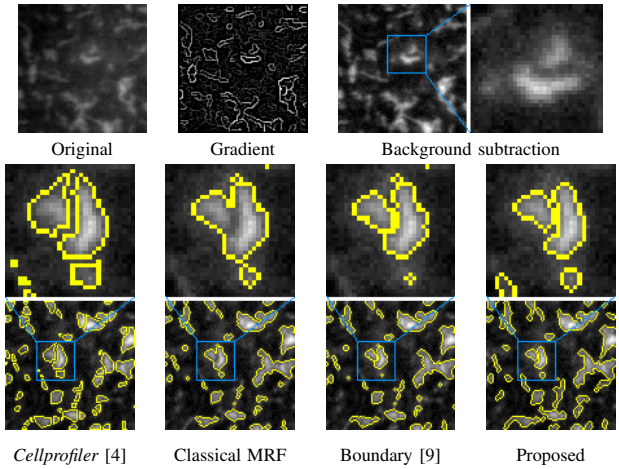


Figure 3. Comparison on a TIRF image.

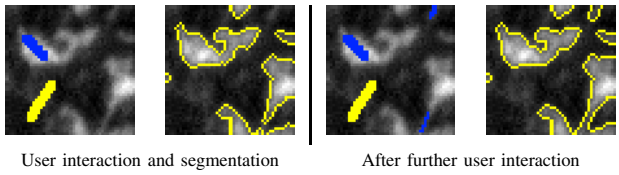


Figure 4. The effect of user interaction.

### A. Application in TIRF microscopy

The proposed approach has also been validated on images taken in Total Internal Reflection Fluorescence (TIRF) microscopy mode, which is an elegant optical technique that provides for the excitation of fluorophores in an extremely thin axial region (optical section) [10]. Images in Fig. 3 and Fig. 5 were taken by a CytoScout fluorescent microscope system using the 488-nm argon-ion laser line for the excitation of fluorescein. They show the plasma membrane of B16 mouse melanoma cells labeled with the fluorescence cholesterol analogue fPEG-Chol which specifically recognizes cholesterol-rich membrane domains [11]. Higher intensity

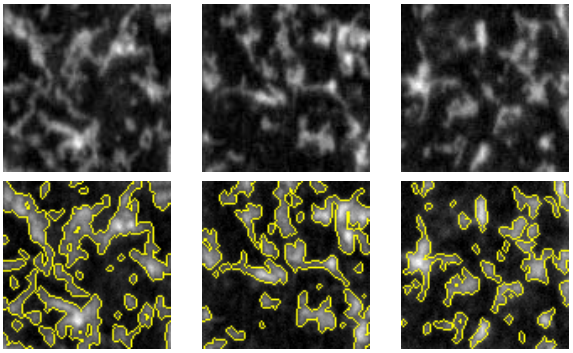

Figure 5. Results on TIRF images.

regions indicate cholesterol-rich membrane rafts, which are signaling platforms in the plane of biological membranes playing important roles in many cellular functions.

The quantitative analysis of these sub-cellular structures requires an accurate segmentation. Due to the rather low contrast, a standard background subtraction (available in Matlab) preprocessing step has been applied before segmentation (see Fig. 3). The user interaction consists in simple mouse operated brush strokes of blue (object) or yellow (for background) as shown in Fig. 4. Based on these samples, the foreground/background Gaussian parameters are computed and an initial segmentation is created. If the segmentation is not accurate, then the user may brush part of a wrongly labeled area. In addition to update the Gaussian parameters, it is also possible to constrain these marked regions either to be firm foreground or firm background, then a new segmentation is generated.

In Fig. 3, we compare results obtained by *Cellprofiler* [4] and classical MRF models. Each method's parameters have been manually fine-tuned to get the best result. Notice that *Cellprofiler* tends to produce rather "blocky" boundaries, while the classical MRF model misses some foreground regions as well as merges nearby regions due to the lack of gradient information. Although the classical MRF model with boundary term [9] achieves slightly better separation, our method clearly provides the most accurate segmentation. We remark that the same watershed-based postprocessing step used in *Cellprofiler* can also be applied in our method to further cut larger regions into smaller patches. Additional results can be seen in Fig. 5. These segmentation results have been validated by expert biologists who found them accurate and relevant. The runtime was consistently below $0.07$ sec on TIRF images of size $100 \times 100$.

## V. Conclusion

We have proposed a novel MRF model which includes edge information while also satisfying the submodularity constraint. Therefore, an exact MAP solution can be obtained via standard max-flow/min-cut within fraction of a second. Quantitative evaluation on synthetic images showed that objects in blurred noisy images can be accurately segmented. The proposed method has been successfully applied in TIRF fluorescence microscopy and compared favorably to state of the art methods.

## References


[1] S. Raman, B. Parvin, C. Maxwell, and M. H. Barcellos-Ho, "Geometric approach to segmentation and protein localization in cell cultured assays," in *Advances in Visual Computing*, Nov. 2005, pp. 427–436.

[2] C. Russell, D. Metaxas, C. Restif, and P. Torr, "Using the $P^n$ Potts model with learning methods to segment live cell images," in *International Conference on Computer Vision*. IEEE, Oct. 2007, pp. 1–8.

[3] C. Chen, H. Li, X. Zhou, and S. T. C. Wong, "Constraint factor graph cutbased active contour method for automated cellular image segmentation in RNAi screening," *Journal of Microscopy*, vol. 230, no. 2, pp. 177–191, May 2008.

[4] T. R. Jones, I. H. Kang, D. B. Wheeler, R. A. Lindquist, A. Papallo, D. M. Sabatini, P. Golland, and A. E. Carpenter, "Cellprofiler analyst: data exploration and analysis software for complex image-based screens," *BMC Bioinformatics*, vol. 9, no. 1, p. 482, Nov. 2008.

[5] S. Geman and D. Geman, "Stochastic relaxation, Gibbs distributions, and the Bayesian restoration of images," *IEEE Transactions on Pattern Analysis and Machine Intelligence*, vol. 6, no. 6, pp. 721–741, Nov. 1984.

[6] V. Kolmogorov and R. Zabih, "What energy functions can be minimized via graph cuts?" *IEEE Transactions on Pattern Analysis and Machine Intelligence*, vol. 26, no. 2, pp. 147–159, Feb. 2004.

[7] Y. Boykov and V. Kolmogorov, "An experimental comparison of min-cut/max-flow algorithms for energy minimization in vision," *IEEE Transactions on Pattern Analysis and Machine Intelligence*, vol. 26, no. 9, pp. 1124–1137, Sept. 2004.

[8] A. Blake, C. Rother, M. Brown, P. Perez, and P. Torr, "Interactive image segmentation using an adaptive GMMRF model," in *European Conference on Computer Vision*, ser. LNCS, T. Pajdla and J. Matas, Eds., vol. 3021, 2004, pp. 428–441.

[9] Y. Boykov and M.-P. Jolly, "Interactive graph cuts for optimal boundary & region segmentation of objects in N-D images," in *International Conference on Computer Vision*, vol. 1, July 2001, pp. 105–112.

[10] K. Fish, "Total internal reflection fluorescence (TIRF) microscopy." *Curr Protoc Cytom*, vol. Chapter 12, 2009.

[11] E. Nagy, Z. Balogi, I. Gombos, M. Akerfelt, A. Bjorkbom, G. Balogh, Z. Torok, A. Maslyanko, A. Fiszer-Kierzkowska, K. Lisowska, P. Slotte, L. Sistonen, I. Horvath, and L. Vigh, "Hyperfluidization-coupled membrane microdomain reorganization is linked to activation of the heat shock response in a murine melanoma cell line," in *Proc. Natl. Acad. Sci. USA*, vol. 104, 2007, pp. 7945–7950.